Energy Storage |*Hot Paper*|

Molecular Solar Thermal Batteries through Combination of Magnetic Nanoparticle Catalysts and Tailored Norbornadiene Photoswitches

Patrick Lorenz[+], Tobias Luchs[+], and Andreas Hirsch*[a]

Abstract: Cobalt catalysts are immobilized on the surface of iron oxide nanoparticles for the preparation of highly active quasi-homogeneous catalysts toward an efficient release of photochemically stored energy in norbornadiene-based photoswitches. The facile separation of the iron oxide nanoparticles through exploitation of the intrinsic magnetic properties of this material enables efficient cyclization of energy storage and release. Through the transition from cobalt (II) salphen to cobalt porphyrins, a 22.6-fold increase in the catalytic efficiency of the QC-NBD back-conversion is achieved, with an initial TOF of up to 3.64 s^{-1} and excellent TON of over 3305. In addition, a series of novel "push–pull" functionalized norbornadiene derivatives is prepared, featuring excellent absorption properties with maxima up to 366 nm, quantum yields around 70%, high energy storage capacities of up to 98.0 kJ mol^{-1}, and outstanding thermal stability with $t_{1/2}$ (25 °C) over 100 days. Finally, the energy storage potential of these molecular solar thermal (MOST) systems is harnessed in a heat release experiment. This demonstrates the potential of norbornadiene-based photoswitches in combination with efficient magnetic catalysts for the generation of environmentally benign process heat.

Introduction

In search of renewable energy sources, the concept of harvesting and storing solar energy in a unimolecular device has recently received increasing attention.[1] Such molecular solar thermal (MOST) energy storage systems have a distinct advantage over common solar-based energy systems, which is that they are not affected by the mismatch between energy availability and energy demand. Within these systems, the harvested sunlight is used to drive a photoisomerization from a low-energy isomer to a metastable energy-rich counterpart. Thereby, the energy is stored in chemical bonds and later released on demand as thermal energy (Scheme 1).[2] Conceivable applications for these solar thermal batteries include not only domestic heating, but also the generation of industrial process heat. The heat used directly in industrial processes to manufacture goods makes up a significant share of the overall industrial energy demand, and to a large extent, low to medium heat is required.[3] Even though industrial process heat and domestic heating account for a large portion of the total energy consumption, they still rely heavily on fossil fuels. Although still in their infancy, green solutions for heating applications such as

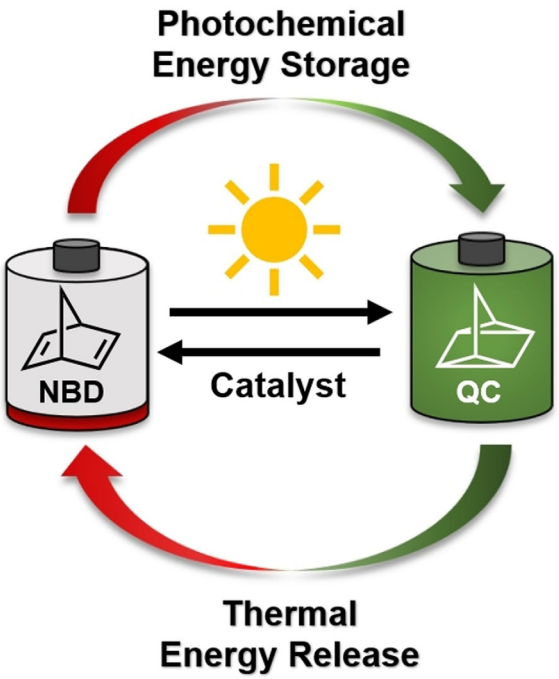

Scheme 1. Schematic representation of a solar thermal battery based on the norbornadiene (NBD)/quadricyclane (QC) photoswitch.

[a] *P. Lorenz,[+] T. Luchs,[+] Prof. Dr. A. Hirsch*
Department of Chemistry and Pharmacy
Institute of Organic Chemistry
Friedrich-Alexander-Universität Erlangen-Nürnberg
Nikolaus-Fiebiger-Strasse 10, 91058 Erlangen (Germany)
E-mail: andreas.hirsch@fau.de

[+] *These authors contributed equally to this work.*

Supporting information and the ORCID identification number(s) for the author(s) of this article can be found under: https://doi.org/10.1002/chem.202005427.

solar thermal collectors and photovoltaic heating are under intensive investigation and are already in application.[4] To bridge the gap between energy demand and the availability of solar energy, thermal energy storage is required. MOST systems are ideal candidates to meet the high and continuous demand of industrial process heat and domestic heating owing to their lack of transformation losses, long storage time, and fast energy release.

Several photoswitches have been investigated with regard to their MOST potential.[5] Despite the diversity of potential candidates, the key requirements for a MOST system are always the same: 1) good absorption properties of the parent molecule across the solar spectrum; 2) little competing absorption of the metastable photoisomer; 3) high quantum yield of the photoisomerization; 4) long half-life of the metastable energy-rich isomer; 5) high energy storage density; and 6) good cyclability.[6]

The best studied[7] and arguably the most promising among MOST candidates is the interconversion system of norbornadiene (NBD) and quadricyclane (QC), shown in Scheme 1. The parent system already combines a huge energy density with the long half-life of QC.[8] Moreover, it has been shown that by introducing substituents into the carbon framework of NBD, it is possible to redshift the absorption into the visible region of the spectrum, and at the same time, increase the quantum yield.[9] However, these beneficial photophysical properties come at the cost of an increased molecular weight and therefore lower energy storage capacities.[10] Optimization of one characteristic of any NBD–QC couple always affects the remaining characteristics as well, rendering the design of the ideal NBD–QC interconversion system a challenging and yet unsolved task. Nevertheless, by performing detailed and systematic investigations, the group of Moth-Poulsen in particular has made considerable progress recently.[11] Next to a tailor-made NBD–QC couple, an efficient and well-designed catalyst is of paramount importance for a practical MOST system.[6a,12] The catalyst must enable on-demand energy release with a sufficient turnover number (TON) and turnover frequency (TOF).

Furthermore, the formation of side products must be ruled out, and the catalyst should be readily separable from the solar fuel to allow easy cyclization of the process. The latter requirement is best met by heterogeneous catalysts; however, in many cases they are inferior to homogeneous catalysts in terms of reactivity and selectivity.[13] By using high-surface-area materials such as magnetic iron oxide nanoparticles (NPs) as the support for a molecular catalyst, the best of both worlds can be achieved. Through the deposition of self-assembled monolayers, the material's properties can be modified to facilitate the encapsulation of apolar molecules,[14] interchangeable dispersibility,[15] drug delivery,[16] or the design of quasi-homogeneous catalysts.[17] Recently, we showed that by anchoring a CoSalphen catalyst onto magnetic Fe_3O_4 NPs, it is possible to adapt this concept for the design of an easily cyclable MOST system.[18] Despite this very successful proof of concept, the huge potential of combining magnetic NP catalysts with the NBD/QC interconversion in a MOST system has, so far, not nearly been exhausted.

In this paper we provide the tools that allow this enormous potential to be harnessed. On the one hand, we have designed new and much more efficient magnetic catalysts. On the other hand, we have synthesized a variety of novel NBD–QC interconversion couples and performed detailed investigations regarding their MOST potential. By studying the kinetics of these magnetic NP-based catalysts, for the first time we were able to show that the second generation, based on cobalt porphyrins as the active catalyst, is far more reactive than the previously reported cobalt salphen **[Fe_3O_4-Cat1]**, which is impressively shown by a 22.6-fold increase in reactivity. This new catalyst generation in combination with the outstanding photophysical properties of the novel NBD–QC couples (λ_{onset} up to 450 nm and $\Phi \approx 70\,\%$) paves the way toward an efficient MOST system utilizing the sunlight-driven isomerization of NBD to QC and a magnetic NP-anchored quasi-homogenous catalyst. Finally, we have investigated the heat release capacity of the nanoparticle-catalyzed back-conversion of **QC1** to **NBD1** in a 1 M solution, yielding a temperature increase to 39.5 °C in a glass vial without insulation. This demonstrates that the generation of low to medium heat for industrial processes as well as domestic heating is a field of application for this MOST concept.

Results and Discussion

We opted to utilize commercially available Fe_3O_4 nanoparticles with a specific surface area of 100 $m^2 g^{-1}$ (derived from BET measurements) as the metal oxide core for the immobilization of catalytically active functional molecules. Previously, we reported that Fe_3O_4 nanoparticles, functionalized with a cobalt (II) salphen moiety carrying a carboxylic acid (**Cat1**) as anchor group, act as an effective magnetic catalyst for the exothermic back-conversion of QC to NBD.[18] On the basis of these results, we improved the nanoparticle functionalization process and expanded it to cobalt tetraphenylporphyrin-based catalysts, which are known to facilitate the QC to NBD interconversion efficiently.[19] **Cat2** is an asymmetric A_3B porphyrin with a single carboxylic acid as anchoring group, whereas **Cat3** is a symmetric A_4 porphyrin carrying four carboxylic acid groups for anchoring on metal oxide surfaces (Scheme 2). For the preparation of the magnetic catalyst, Fe_3O_4 nanoparticles were treated with 10 wt% of the respective cobalt complex (**Cat1**, **Cat2**, or **Cat3**) in isopropanol (Scheme 2). The resulting dispersions were subsequently irradiated by tip sonication for 30 min and then stirred under ambient conditions for 48 h. After centrifugation, the reduced color in the supernatant indicated immobilization of the cobalt complexes on the NPs. The resulting NP hybrids **[Fe_3O_4-Cat1–3]** were submitted to multiple washing steps consisting of redispersion in isopropanol and centrifugation to remove any unbound ligands. Finally, a washing step with separation induced by an external magnet instead of centrifugation was conducted. After oven drying, the catalyst loading was determined by elemental analysis. Loadings of 7.9 wt% catalyst for **[Fe_3O_4-Cat1]**, 3.9 wt% for **[Fe_3O_4-Cat2]**, and 7.4 wt% for **[Fe_3O_4-Cat3]** were determined (Supporting Information).

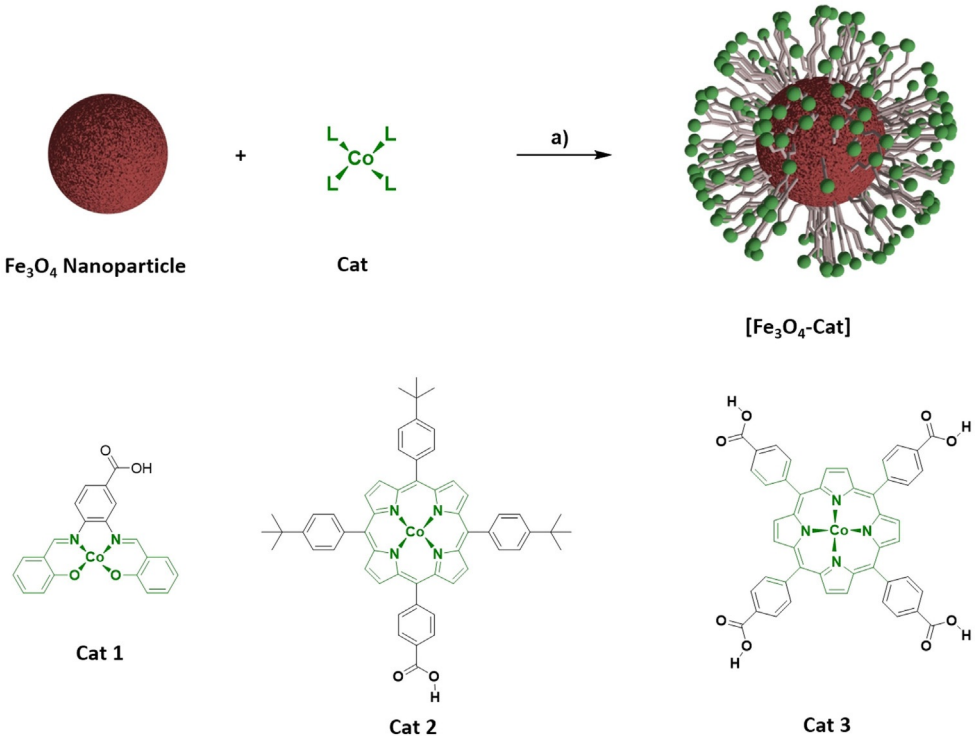

Scheme 2. Functionalization of iron oxide nanoparticles with three different catalytically active molecules **Cat1**, **Cat2**, and **Cat3**. a) Isopropanol, 30 min sonication, 48 h rt.

To establish the best possible energy storage and release system, next to this new generation of magnetic NP-based catalysts, we also synthesized NBD–QC couples with exceptional half-lives, redshifted absorption profiles, outstanding quantum yields, and high energy storage capacity. For this purpose, we synthesized a library of NBD derivatives and investigated them regarding their potential as MOST candidates. Considering our encouraging experience with the previously published interconversion couple **NBD1/QC1**,[18] we planned to synthesize structurally similar NBD derivatives, but with superior photophysical properties. One way to redshift the absorption profile of such derivatives, which has been used widely by the group of Moth-Poulsen, is the amplification of the push–pull effect.[10,20] Using this knowledge, we decided to attach electron-donating groups (EDGs) to the phenyl ring of **NBD1**. The synthesis of derivatives **NBD2**–**5** was achieved through two different strategies as depicted in Scheme 3. The NBD derivatives **NBD2**–**4** were synthesized in an effective transition-metal-free Corey–Fuchs reaction from aldehyde precursors toward a push–pull alkyne equipped with a carboxylic ester and a suitably substituted phenyl ring (pathway A). The alkyne precursors of **NBD2**–**4** were synthesized in good overall yields, and the alkyne precursor of **NBD1** is also commercially available. These alkynes were then further subjected to a [4+2] Diels–Alder reaction with cyclopentadiene under microwave irradiation at 180 °C to yield the desired norbornadiene derivatives **NBD1**–**4.** **NBD5** was synthesized according to pathway B: iodination of *N*,*N*-dimethylaniline gave 4-iodo-*N*,*N*-dimethylaniline, which was reacted with methyl propiolate in a Negishi reaction. This alkyne was then subjected to a Diels–Alder reaction with cyclopentadiene to give the desired product **NBD5**. To test our new magnetic catalysts toward sterically more demanding derivatives, we designed and synthesized **NBD6** (Scheme 3, pathway C). Because of the six methyl groups in combination with the two ester moieties, the inner carbon framework of **NBD6** and the corresponding **QC6** is sterically well shielded. This could potentially hamper the coordination of **QC6** to the active site of the catalyst and therefore slow down or even prevent the back-reaction. Besides the steric hindrance, **NBD6** also differs from the other NBD derivatives by the mechanism underlying the photoisomerization. As mentioned above, **NBD1**–**5** are all push–pull substituted NBD derivatives, whereas **NBD6** can be regarded a so-called charge-transfer NBD. These NBD derivatives distinguish themselves by having one electron-rich and one electron-poor double bond.[6a] Owing to the close proximity of the two double bonds in NBD and the resulting through-space interaction, the characteristic charge-transfer band occurs in the UV/Vis region.[6a,21] Irradiation of this band results in the formation of the corresponding QC derivatives.[6a,21a]

With this library of new NBD derivatives at hand, the next step was to test them regarding their potential as MOST candidates. Whether or not an NBD/QC couple is suitable for MOST applications depends on several criteria, which will be determined and discussed in the following section. As already mentioned, one of the key requirements for a MOST system is a good spectral overlap between the absorption spectrum of the parent molecule and the solar spectrum. Figure 1 shows the photoisomerization of **NBD1**–**6** (blue line) toward their corresponding QC derivatives (red line) followed by UV/Vis spec-

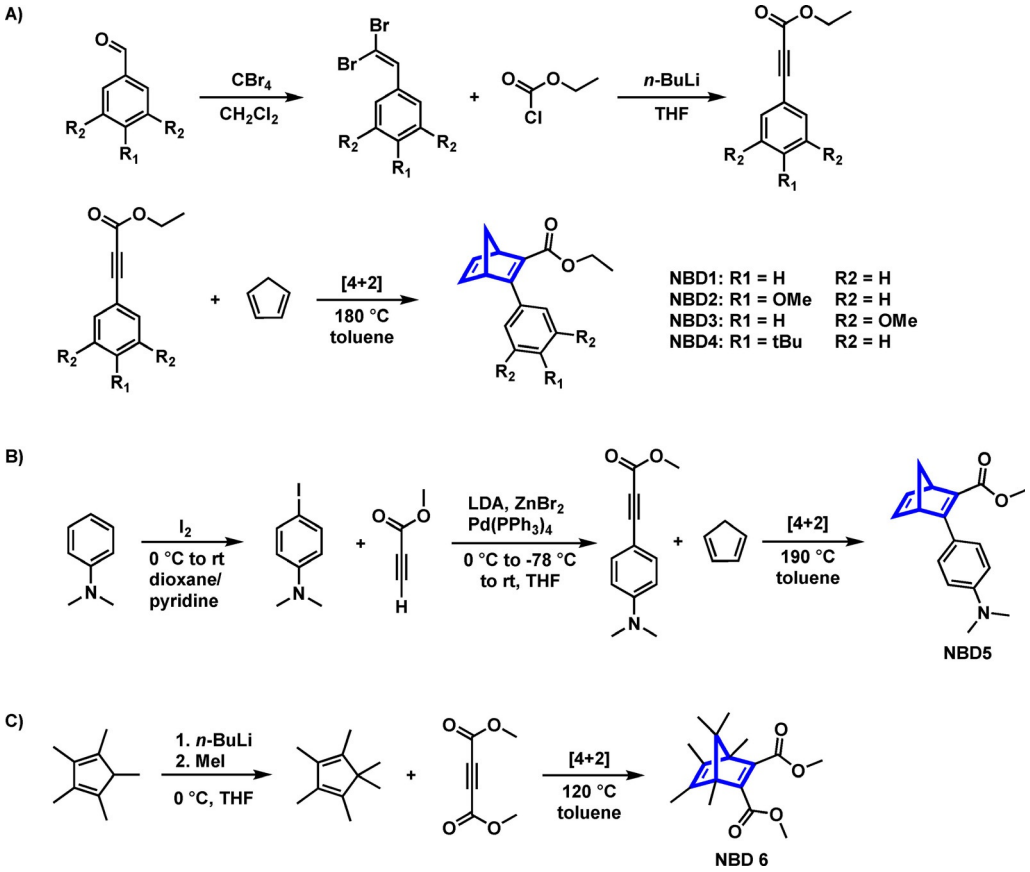

Scheme 3. Synthetic pathways toward the functionalized NBD derivatives **NBD1**–**6**. Pathway A relies on the Corey–Fuchs reaction to prepare the alkyne species, which is required for the Diels–Alder reaction with Cp towards the final push–pull NBD derivatives **NBD1**–**4**. Pathway B involves a Negishi coupling to obtain the desired alkyne precursor, followed by a Diels–Alder reaction. Pathway C involves methylation of pentamethylcyclopentadiene followed by a Diels–Alder cycloaddition to yield the charge-transfer derivative **NBD6**.

troscopy. Therefore, a quartz glass cuvette was charged with a solution of the respective parent **NBD1**–**4**, **NBD6** in acetonitrile, or **NBD5** in benzene, and irradiated at 310 nm and 365 nm, respectively, until no further change in the absorption profile could be detected, indicating full conversion. (Since photoisomerization of **NBD5** to **QC5** in polar solvents is more complicated than for the other NBD/QC couples, less polar solvents such as toluene and benzene were chosen for this reaction). As expected, a significant redshift of the absorption profile compared with unfunctionalized NBD ($\lambda_{onset} < 267$ nm)[10] can be observed for all derivatives. For the push–pull NBD derivatives **NBD1**–**5**, this redshift of the low-energy absorption maximum is in line with the strength of the electron-donating group attached to the phenyl ring (**NBD1** < **NBD4** ≈ **NBD3** < **NBD2** < **NBD5**), with only **NBD3** falling out of this sequence owing to the substituents being bound in *meta* position. In case of the donor–acceptor **NBD6**, the low-energy absorption band is centered around 311 nm and assigned to the characteristic charge transfer between the electron-rich and the electron-poor double bonds of donor–acceptor NBDs.[6a,21a] The existence of at least one isosbestic point in all of the monitored photoisomerizations indicates a clean conversion of **NBD1**–**6** to the corresponding QCs. This was corroborated by NMR experiments, which not only confirmed the absence of any side products, but also showed full conversion in all cases (see Supporting Information). Upon comparing the absorption profiles of the NBDs (blue line) with the corresponding QCs (red line), a significant blueshift upon transformation can be observed for all derivatives, enabling selective photoisomerization of the NBDs.

With an absorption maximum at 366 nm ($\varepsilon =$ 17490 $M^{-1}cm^{-1}$) and an absorption onset of 450 nm, **NBD5** already matches the high-energy portion of the solar spectrum quite well. This encouraged us to test the photoisomerization of **NBD5** to **QC5** directly driven by sunlight. For this purpose, a quartz glass cuvette was filled with **NBD5** (5.0 mg) dissolved in deuterated toluene (3.0 mL) and exposed to direct sunlight on the windowsill. Already after five minutes, the color of the solution had changed from yellow to colorless, indicating isomerization to **QC5**. An aliquot was taken for ^{1}H NMR analysis, and from the integral ratio of the signals a **NBD5**/**QC5** ratio of 5:95 % was estimated. After another five minutes of exposure to sunlight the conversion to **QC5** was complete, and remarkably, no side products were observed (for more details see Supporting Information). This impressively illustrates the outstanding photophysical properties of this NBD/QC couple.

Apart from the overlap with the solar spectrum and the extinction coefficients, the quantum yield of the respective pho-

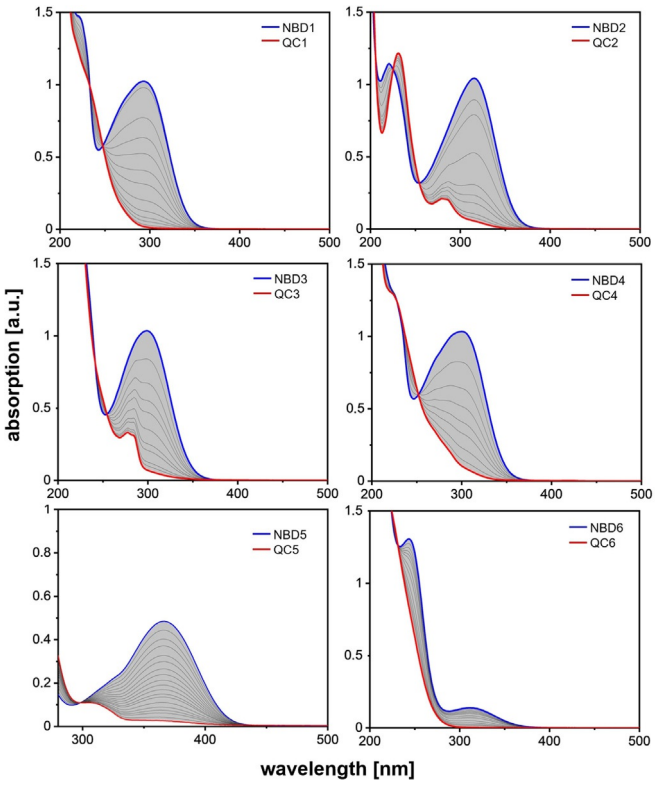

Figure 1. UV/Vis absorption spectra of **NBD1–6** during photoisomerization. **NBD1–4** and **NBD6** were irradiated at 310 nm in acetonitrile, whereas **NBD5** was irradiated at 365 nm in benzene. The characteristic absorption features of the NBD moieties (blue line) show a rapid decline during the irradiation process. Distinct isosbestic points in each measurement indicate a clean conversion of each NBD to its energy-rich isomer. The absorption profiles of the resulting QCs **QC1–6** (red-line) are significantly blueshifted relative to their NBD forms.

toisomerization is needed to further quantify the energy storage efficiency. The quantum yields of the reactions **NBD1–6** to **QC1–6** were determined by using potassium ferrioxalate as chemical actinometer,[22] and are presented in Table 1. For this purpose, **NBD1–4** and **NBD6** were dissolved in acetonitrile and irradiated with 310 nm light, whereas **NBD5** was dissolved in toluene and irradiated at 365 nm (for more information see Supporting Information). The obtained values for the quantum yields vary between 51% for **NBD5** and 82% for **NBD6**. However, both values have to be treated carefully; owing to the low extinction coefficient of **NBD6**, quite a concentrated solution was necessary to guarantee an optically thick solution. In the case of **NBD5** a concentration dependence of the quantum yield was observed whereby higher concentrations gave higher quantum yields; however, a saturation of the obtained quantum yield was detected at the reported value of 51% (for more details see Supporting Information).

Another important characteristic of every NBD/QC couple is its energy storage density. The enthalpies of the thermal back-reaction were determined by performing differential scanning calorimetry (DSC) experiments with **QC2–6** (Figures S1–S11, Supporting Information). As an example, Figure 2 depicts the obtained DSC curves of **QC2** (top) and **QC5** (bottom). In every case a strong exothermic peak was observed in the first heating cycle, which can be assigned to the thermal back-reaction. The absence of this peak in the second heating cycle proves that the transformation of QC to NBD was completed within the first heating cycle. In the case of the **NBD5**/**QC5** couple, two peaks can be observed in the second heating cycle, which are assigned to phase transformations of **NBD5**. The absence of any side reactions was proven by ^{1}H NMR analysis after completion of the DSC experiments (for more details see Supporting Information). The measured enthalpies vary between 75.0 and 98.0 kJ mol^{-1}, and in combination with the molecular weight of the respective NBD/QC couple these correspond to energy storage densities between 249.7 and 367.5 kJ kg^{-1} in the neat systems.

As well as the amount of energy that can be stored within the metastable QC derivatives, their kinetic stability is also of paramount importance as it determines the timespan over which the energy can be stored. The thermal half-life of QC derivatives at room temperature can vary considerably between a few hours and years.[10,20,23] To determine the thermal half-life of **QC2,4,5**, we prepared stock solutions of the respective NBDs in deuterated tetrachloroethane (**NBD2,4**) or deuterated toluene (**NBD5**) and irradiated them with 310 and 365 nm light, respectively, until ^{1}H NMR indicated full conversion. By

Table 1. Summary of the optical and thermodynamic properties of the interconversion couples **NBD1–6**/**QC1–6**. $t_{1/2}$ (25 °C) determined in deuterated tetrachloroethane (**QC1**, **QC2** and **QC4**) or in deuterated toluene (**QC5**). The optical parameters λ_{max}, λ_{onset}, and ε_{max} were determined from UV/Vis spectra in acetonitrile (**NBD1–4** and **NBD6**) or toluene (**NBD5**). ΔH as determined from the average of at least two DSC measurements. Quantum yields for the photoisomerization in acetonitrile (**NBD1–4** and **NBD6**) or toluene (**NBD5**) determined from at least two independent measurements, according to a literature-known method.[22]

NBD Derivative	MW [g mol^{-1}]	$t_{1/2}$ (25 °C) [days]	λ_{max} [nm]	λ_{onset}[a] [nm]	ε_{max} [M^{-1} cm^{-1}]	ΔH [kJ mol^{-1}]	ΔH [kJ kg^{-1}]	Φ_{isom} [%]
NBD1	240.30	450[b]	291	359	6460	88.3 ± 0.2[b]	367.5 ± 0.8 [b]	71
NBD2	270.33	156	316	380	10780	87.4 ± 0.4	323.3 ± 1.5	68
NBD3	300.35	/	299	364	7500	75.0 ± 0.2	249.7 ± 0.7	73
NBD4	296.41	611	300	370	8680	77.3 ± 0.2	260.8 ± 0.7	59
NBD5	269.34	103	366	450	17490	98.0 ± 0.4	363.9 ± 1.5	51[c]
NBD6	292.38	/	311	357	420	/	/	82[d]

[a] λ_{onset} is defined as the wavelength with $\log(\varepsilon) = 2$. [b] Values adapted from ref. [18]. [c] The quantum yield of **NBD5** increased in line with the concentration, reaching a saturation at 51% (for more details see Supporting Information). [d] Owing to the low extinction coefficient of **NBD6**, a quite concentrated solution was necessary to obtain an optically thick solution.

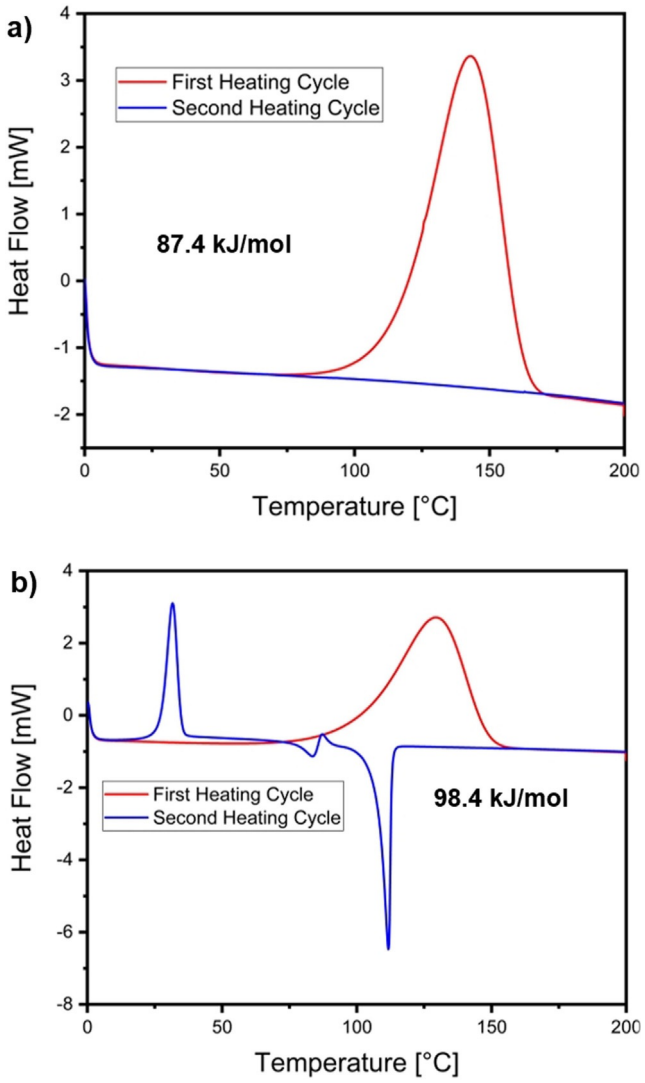

Figure 2. a) DSC measurement of **QC2**. The peak during the first heating cycle is strongly exothermic and can be assigned to the back-conversion of **QC2** to **NBD2** corresponding to a heat release of 87.4 kJ mol^{-1}. b) DSC measurement of **QC5**. The peak in the first heating cycle is exothermic and can be assigned to the back-conversion of **QC5** to **NBD5** corresponding to a heat release of 98.0 kJ mol^{-1}. The two other peaks in the second heating are assigned to phase transformations after the rapid cooling process.

following the thermal back-reaction of the thus-prepared QCs directly by NMR, it was possible to estimate the rate constants k of each QC derivative at different temperatures. These parameters in combination with the Eyring equation enabled us to calculate $\Delta H^{\#\#}_{thermal}$ and $\Delta S^{\#\#}_{thermal}$ (see Supporting Information). Furthermore, through extrapolation of the data, we determined the half-life of **QC2**,**4**,**5** at 25 °C (Table 1). With $t_{1/2}$ (25 °C) between 103 and 611 days, all the QCs reported here are suitable for long-term energy storage. Compared with the photochemical characteristics of other literature-known NBD derivatives, our compounds are highly competitive; in particular, **NBD5** combines an exceptional absorption profile with high thermal stability.[11a]

After an in-depth analysis of the optical and thermodynamic properties of each NBD/QC couple we focused on the catalytic back-conversion of the metastable QC isomers to their NBD form. For a well-performing MOST device, a controlled and fast release of the photochemically stored energy is of paramount importance. Further, a facile removal of the applied catalytic materials is crucial to ensure a functioning cycle of solar-driven energy storage followed by on-demand energy release, triggered by the catalyst. Owing to their intrinsic magnetic properties, the nanoparticle hybrids **[Fe_3O_4-Cat1–3]** allow easy purification through the application of an external magnet. Additionally, we investigated these nanoparticle hybrids on their catalytic activity for the back-conversion of QC to NBD. For this purpose, **NBD1** (8.66×10^{-2} mmol) dissolved in $CHCl_3$ was irradiated (310 nm) for approximately 2 h until complete conversion to **QC1** was achieved. This was verified by peak integration of HPLC measurements. The resulting solution of **QC1** was then treated with 0.3 mg of the magnetic nanoparticle catalysts **[Fe_3O_4-Cat1–3]**. After addition of the catalyst particles, the reaction mixtures were mixed on a vibrating plate, and after set time intervals, the catalyst particles were sedimented with an external magnetic field and aliquots of the mixture were taken for HPLC analysis. These investigations revealed a very slow QC–NBD back-conversion rate for the first-generation catalyst particles **[Fe_3O_4-Cat 1]**. Under the applied reaction conditions, a **QC1**–**NBD1** conversion of 5% was reached after 3 h. As described previously, an increase in the concentration of **[Fe_3O_4-Cat1]** led to complete conversion.[18]

As evident from Figure 3, a tremendous increase in catalyst performance was observed upon using the second generation of porphyrin-based catalysts **[Fe_3O_4-Cat2–3]**. Both nanoparticle hybrids displayed a very high initial activity compared with **[Fe_3O_4-Cat1]**, with **[Fe_3O_4-Cat2]** facilitating complete conversion of **QC1** to **NBD1** after only 40 min (Figure 3).

However, after separation of the catalyst particles **[Fe_3O_4-Cat2]**, the supernatant displayed a yellow color, which indicated desorption of the porphyrin ligand **Cat2** from the nanopar-

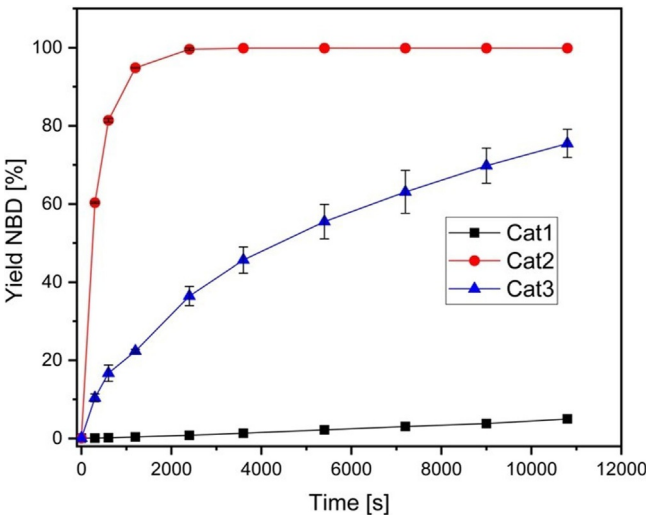

Figure 3. Comparison of the catalytic effectivity of the three magnetic nanoparticle catalyst systems **[Fe_3O_4-Cat1–3]** in the back-conversion of **QC1** to **NBD1** in chloroform. The conversion of **QC1** to **NBD1** was followed by HPLC analysis.

ticle surface. UV/Vis analysis later suggested the presence of the dication of the free base porphyrin ligand **Cat2** (Supporting Information). Thus, the high excess of **QC1**/**NBD1** led to desorption and degradation of **[Fe_3O_4-Cat2]**. In contrast, **[Fe_3O_4-Cat3]** also displayed a high initial activity and resulted in a **QC1**–**NBD1** back-conversion of 75% after 3 h, without showing any signs of desorption from the surface. Through this combination of high activity and stability against desorption we deemed **[Fe_3O_4-Cat3]** to be the most suitable catalyst candidate. The initial turnover frequency (TOF) after 5 min was calculated at 1.15 s^{-1}. This corresponds to a 22.6-fold increase in activity compared with the first-generation catalyst **[Fe_3O_4-Cat1]** reported previously [TOF (5 min): 0.0508 s^{-1}].[18]

We decided to utilize **[Fe_3O_4-Cat3]** as the catalyst system for all further investigations on the library of QC molecules **QC1**–**6**, owing to the very stable anchoring and extremely high activity compared with the other catalyst candidates. Therefore, solutions of each NBD derivative were irradiated with a UV-LED setup either at 310 nm in chloroform for **NBD1**–**4** and **NBD6** or at 365 nm in toluene for **NBD5**. The samples were irradiated until complete conversion to the metastable QC form was verified by HPLC analysis for the NBD-QC couple **1** or NMR analysis for the NBD-QC couples **2**–**6**. After the successful photoisomerization, **QC2**–**6** (1.44×10^{-2} mmol) dissolved in the respective solvent (0.5 mL) was treated with the magnetic nanoparticle catalyst **[Fe_3O_4-Cat3]** (0.05 mg) dispersed in the corresponding solvent (50 μL). The resulting dispersions were then mixed on a vibrating plate. After set time intervals, the nanoparticle catalyst was sedimented by using an external magnetic field and the supernatant was removed for analysis. For each sample, the conversion ratio of QC to NBD was monitored by comparing the integrals from the NMR analysis (conversion values for **NBD1** were determined by HPLC and taken from Figure 3). The results were then plotted versus the exposure time of each sample to the nanoparticle catalyst (Figure 4). In addition to the depicted time intervals, the QC-NBD conversion was also recorded after an exposure time of 3 h.

Figure 4 displays some key differences between the NBD derivatives. Most notable was the difference in catalytic QC-NBD back-conversion activity that resulted from the chemical modifications to the electron-donating phenyl substituent. In general, the presence of these electron-donating groups increased the back-conversion activity of **QC2**–**4** substantially.

In **QC5** however, we observed a reduced back-conversion activity. On the one hand, this can be attributed to the change of the solvent. On the other hand, this reduced activity may be a result of coordination of the amine groups of **QC5** to the cobalt centers in **[Fe_3O_4-Cat3]**. Hence, the addition of the labile QC bonds to the cobalt center is hampered, resulting in a reduced effectivity of **[Fe_3O_4-Cat3]** for back-conversion of **QC5**. This correlates well with the observed initial activity, which is reduced significantly after reaction times longer than 5 min (Figure 4). **QC6** did not show any activity in the nanoparticle-mediated back-conversion of the metastable QC form to **NBD6**. We attribute this inactivity to the increased steric bulk, which inhibits coordination to the surface-bound catalytic centers in the magnetic catalyst **[Fe_3O_4-Cat3]**. A similar observation was made by Maruyama et al. using methyl-decorated QC derivatives.[24]

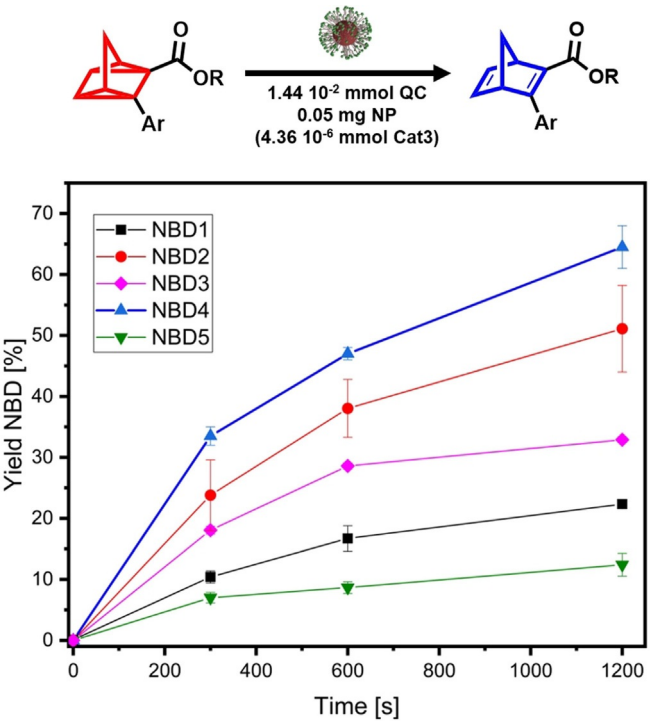

Figure 4. Catalytic back-conversion of **QC1**–**5** to **NBD1**–**5**, mediated by **[Fe_3O_4-Cat3]** (0.03 mol% active catalyst). The conversion of **QC1**–**4** to **NBD1**–**4** took place in chloroform and was followed by HPLC for **NBD1** and by ^{1}H NMR analysis for **NBD 2**–**4**, whereas the conversion of **QC5** to **NBD5** took place in deuterated toluene and was followed by ^{1}H NMR analysis.

To quantify the catalytic activity of the magnetic nanoparticle catalyst **[Fe_3O_4-Cat3]** with each QC derivative, we calculated the turnover frequency (TOF) after 5 min and the turnover number (TON) of the nanoparticle catalyst after a maximum reaction time of 3 h. The TON is calculated as the moles of converted analyte divided by the moles of catalyst used, whereas TOF is defined as TON per second. The interconversion couple **NBD4**-**QC4** displayed the highest initial TOF of 3.64 s^{-1} with a minimum TON of 3305 after complete back-conversion of **QC4** to **NBD4**. We observed the second highest TOF value of 2.62 s^{-1} for the back-conversion of **QC2** to **NBD2** with a very high TON value of 3123 after a reaction time of 3 h. The back-conversion of **QC3** to **NBD3** displayed a slightly reduced initial TOF of 2.11 s^{-1}; however, after reaction times longer than 10 min, a reduced activity was detected, resulting in a TON of 2412 after 3 h exposure to the catalyst particles. **QC1**, featuring an unmodified phenyl ring as donor group, showed, on the one hand, a reduced initial TOF of 1.15 s^{-1}, but on the other hand, a more stable conversion rate. Despite the lower initial activity compared with **QC3**, this resulted in a higher TON of 2496 after a reaction time of 3 h. The lowest QC to NBD back-conversion activity was measured for **QC5**, with a moderate initial TOF of 0.95 s^{-1}. This initial activity rapidly declined, resulting in the lowest TON of 641 after 3 h exposure to the nanoparticle catalyst **[Fe_3O_4-Cat3]**. As discussed above, this lowered activity can be explained either by solvent effects or by inhibi-

tion of the catalyst through coordination of the amine group. After catalytic back-conversion and magnetic separation of the catalyst particles, **NBD1**–**5** could undergo further quantitative steps of photoisomerization and catalytic back-conversion. For **NBD5**, we additionally verified that the photoisomerization quantum yield does not change after treatment with the magnetic nanoparticle catalyst **[Fe_3O_4-Cat3]**.

In particular, the unsubstituted parent NBD-QC interconversion couple holds great potential for an efficient MOST device. Its low molecular weight, combined with the fact that both NBD and QC are pumpable liquids, enables the usage of neat NBD/QC, and therefore, very high gravimetric energy densities. These benefits are to some extent hampered by the fact that the parent NBD does not absorb light above 267 nm.[10] Therefore, a triplet photosensitizer is necessary to facilitate the light-induced isomerization of unsubstituted NBD to the energy-rich QC.[8a,25] During this work, we opted to utilize acetophenone as a photosensitizer. Generally, a solution of NBD and acetophenone in acetonitrile was irradiated with a mercury vapor lamp.

The progress of the photoisomerization was monitored by GC/MS measurements. After a conversion of more than 80% was achieved, QC was collected by fractioned distillation. For investigation of the details of the catalyzed back-conversion of QC to NBD, purified QC (20 μL) was dissolved in either chloroform or acetonitrile and then treated with the nanoparticle catalyst **[Fe_3O_4-Cat3]** (2.0 mg) (Figure 5).

As described previously, these solutions were then mixed on a vibrating plate, and after set intervals the nanoparticle catalyst was removed by an external magnet and aliquots of the solution were taken for analysis by GC/MS. In addition to its limited optical properties, the unsubstituted NBD-QC interconversion couple is a special challenge for the catalytic back-conversion because the QC isomer is relatively stable and has a higher activation barrier for the back-conversion than the vast majority of substituted derivatives. Despite this, the nanoparticle catalyst **[Fe_3O_4-Cat3]** facilitated complete conversion of QC to NBD in both chloroform and acetonitrile as solvent. However, we could observe a solvent-dependent difference in the speed of the back-conversion. In acetonitrile the back-conversion was significantly slower, which is probably a result of the stronger competing coordination of acetonitrile compared with chloroform to the cobalt catalyst,[26] as well as an influence of the solvent on the isomerization itself. The latter trend was also observed for several substituted derivatives of NBD by Moth-Poulsen and co-workers.[27] In general, less polar solvents appear to be more suitable for the fast and on-demand release of the photochemically stored energy.

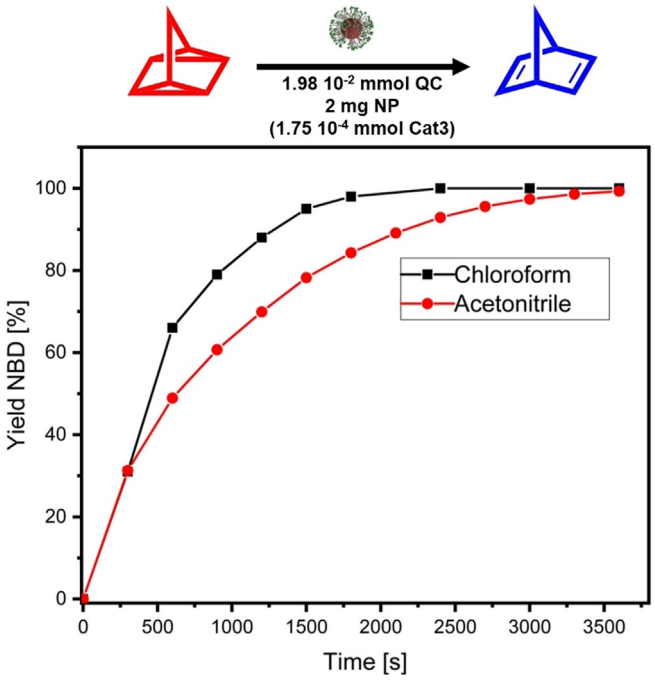

Figure 5. Catalytic back-conversion of unsubstituted quadricyclane to norbornadiene induced by **[Fe_3O_4-Cat3]** nanoparticles, followed by GCMS analysis.

Translation of the stored energy into a practically usable heat release is of paramount importance for the application of MOST devices. On a theoretical level, the achievable temperature rise can be calculated by factoring in the key properties of the storage molecule and solvent through Equation (1).[2]

$$\Delta T = \frac{cMW\Delta H}{(cMWC_{p\_NBD}) + (C_{p\_solv}\rho_{solv})} \quad (1)$$

In this case, *MW* and *c* are the molar weight of the norbornadiene derivative and the concentration, and ΔH is the measured energy storage capacity of the respective QC in $J\,g^{-1}$. For $C_{p\ NBD}$, the heat capacity of NBD, we assumed the value known for the unsubstituted parent norbornadiene ($1.66\,J\,g^{-1}\,K^{-1}$). In the case of **NBD1**, the energy storage capacity is $367\,J\,g^{-1}$. This translates to a theoretical maximum temperature rise of 221 °C without solvent. In a 1 M solution in chloroform this capacity is reduced to a theoretical temperature increase of 48.5 °C. Reaching these theoretical maxima under experimental conditions requires a high degree of engineering to avoid losses from insufficient insulation. Through utilization of a UHV design and a fixed bed catalyst, Moth-Poulsen and co-workers have recently demonstrated that these high theoretical values can be reached with sufficient insulation.[12]

In this work, we demonstrate the heat release potential of 10 mL of a 1 M solution of the interconversion couple **NBD1**-**QC1** in chloroform under ambient conditions in a standard glass vial without any thermal insulation (Figure 6).

Upon addition of the solution of **QC1** to 50 mg of the magnetic nanoparticle catalyst **[Fe_3O_4-Cat3]**, an immediate temperature increase was measured. Within 129 s, the temperature of the solution increased from 24 °C to its peak at 39.5 °C. After reaching its peak the temperature stayed above 30 °C for several minutes. This converts to a total temperature increase of 15.5 °C, which could be achieved without thermal insulation in a 1 M solution of the interconversion couple **NBD1**-**QC1** through catalysis by the magnetic nanoparticle hybrid **[Fe_3O_4-Cat3]**.

After the temperature fell below 30 °C the nanoparticle catalyst was separated from the solution by application of an external magnetic field and the isomerization progress was moni-

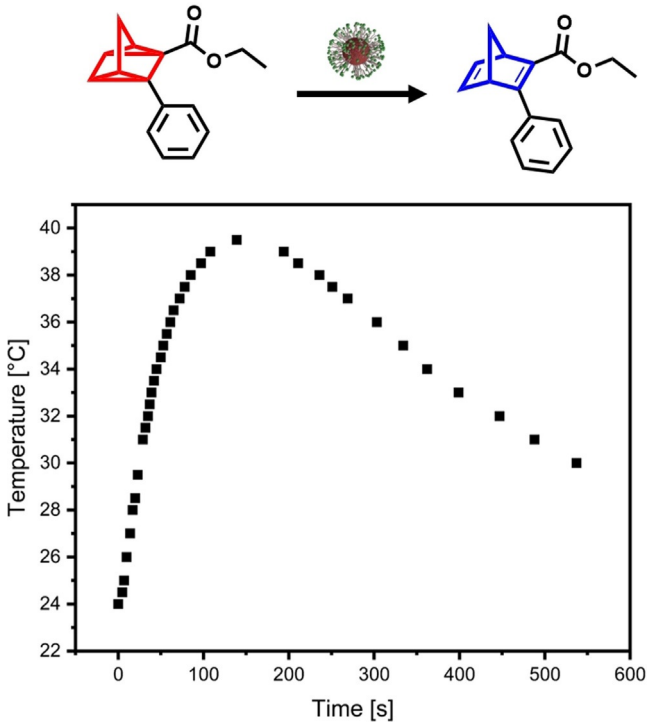

Figure 6. Time-dependent temperature profile of the conversion of a macroscopic amount of **QC1** in $CHCl_3$ (1 M, 10 mL) to **NBD1** catalyzed by **[Fe_3O_4-Cat3]** nanoparticles.

tored by NMR spectroscopy. The ^{1}H NMR analysis showed complete conversion of the 1 M solution of **QC1** to **NBD1** within the reported timespan alongside an effective and facile separation of the catalyst.

Conclusions

In summary, we have developed a highly efficient MOST battery through the combination of NBD photoswitches and a cobalt porphyrin catalyst anchored to magnetic NPs. A stable binding to the nanoparticles surface is achieved through multiple carboxylate anchors, preventing desorption of the active species. For the first time, a detailed analysis of the performance of these novel magnetic NP catalysts was conducted. The high catalytic activity enabled a fast and on-demand release of the photochemically stored energy together with facile magnetic separation of the catalyst particles. In particular, we have significantly improved on our previous work on the combination of a magnetic cobalt salphene catalyst and the interconversion couple **NBD1/QC1**.[18] On the one hand, the interconversion couple **NBD1/QC1** was complemented by a library of NBD/QC derivatives carrying electron-donating groups on the phenyl ring. This led to a significant improvement in their photophysical properties, culminating in facile sunlight-driven conversion of **NBD5** to **QC5**. On the other hand, detailed quantitative experiments on the photochemical properties and catalyst performance were conducted. For the latter, we additionally anchored the two cobalt porphyrins **Cat2** and **Cat3** onto Fe_3O_4 NPs, thereby generating two new and highly efficient magnetic catalysts **[Fe_3O_4-Cat2]** and **[Fe_3O_4-Cat3]**. Desorption and degradation were major issues with **[Fe_3O_4-Cat2]**, but this problem was solved through multiple carboxylate anchors in **[Fe_3O_4-Cat3]**. With this second generation of magnetic NP-based catalysts, we achieved a 22.6-fold increase in catalyst performance compared with the first catalyst generation. **[Fe_3O_4-Cat3]** was tested toward all NBD/QC couples reported herein, and showed excellent performance with an initial TOF up to 3.64 s^{-1} and a TON of more than 3305. However, a solvent dependency of the catalyst performance was observed, whereby a more polar and coordinating solvent seemed to hamper the catalyst performance. Furthermore, we tested the applicability of **[Fe_3O_4-Cat3]** combined with **NBD1/QC1** in a heat release experiment to model its MOST potential. Remarkably, a temperature increment of 15.5 °C was reached without any thermal insulation. This demonstrates that an NBD/QC-based MOST system together with magnetic Fe_3O_4 NP catalysts is, in principle, suitable for applications such as the generation of industrial process heat or domestic heating.

Acknowledgements

We gratefully thank the German Research Council (DFG) for funding through project 391585168 "Photochemisch und magnetochemisch ausgelöste Speicherung/ Freisetzung von Sonnenergie in gespannten organischen Verbindungen". Additionally, we would like to thank the Bavarian Collaborative Research Project Solar Technologies go Hybrid (SolTech), the Cluster of Excellence "Engineering of Advanced Materials" (EAM), funded by DFG, the Graduate School Molecular Science (GSMS), and the Graduate School Advanced Materials and Processes (GSAMP) for financial support. Open access funding enabled and organized by Projekt DEAL.

Conflict of interest

The authors declare no conflict of interest.

Keywords: magnetic catalysts · nanoparticles · norbornadiene · process heat · solar energy storage

[1] a) P. Lorenz, A. Hirsch, *Chem. Eur. J.* **2020**, *26*, 5220 – 5230; b) F. Waidhas, M. Jevric, L. Fromm, M. Bertram, A. Görling, K. Moth-Poulsen, O. Brummel, J. Libuda, *Nano Energy* **2019**, *63*, 103872; c) M. Mansø, A. U. Petersen, K. Moth-Poulsen, M. B. Nielsen, *Org. Biomol. Chem.* **2020**, *18*, 2113 – 2119; d) F. Waidhas, M. Jevric, M. Bosch, T. Yang, E. Franz, Z. Liu, J. Bachmann, K. Moth-Poulsen, O. Brummel, J. Libuda, *J. Mater. Chem. A* **2020**, *8*, 15658 – 15664; e) M. Bertram, F. Waidhas, M. Jevric, L. Fromm, C. Schuschke, M. Kastenmeier, A. Görling, K. Moth-Poulsen, O. Brummel, J. Libuda, *J. Chem. Phys.* **2020**, *152*, 044708; f) K. Ishiba, M.-a. Morikawa, C. Chikara, T. Yamada, K. Iwase, M. Kawakita, N. Kimizuka, *Angew. Chem. Int. Ed.* **2015**, *54*, 1532 – 1536; *Angew. Chem.* **2015**, *127*, 1552 – 1556.
[2] K. Moth-Poulsen, D. Ćoso, K. Börjesson, N. Vinokurov, S. K. Meier, A. Majumdar, K. P. C. Vollhardt, R. A. Segalman, *Energy Environ. Sci.* **2012**, *5*, 8534 – 8537.
[3] a) S. Hess in *Renewable heating and cooling. Technologies and applications, Woodhead Publishing series in energy, number 89*, Ed. G. Stryi-Hipp,

Elsevier, Amsterdam, **2016**, pp. 41 – 66; b) S. Kalogirou, *Appl. Energy* **2003**, *76*, 337 – 361.
[4] a) C. A. McMillan, M. Ruth, *Appl. Energy* **2019**, *239*, 1077 – 1090; b) C. A. Schoeneberger, C. A. McMillan, P. Kurup, S. Akar, R. Margolis, E. Masanet, *Energy* **2020**, *206*, 118083.
[5] a) C.-L. Sun, C. Wang, R. Boulatov, *ChemPhotoChem* **2019**, *3*, 268 – 283; b) A. Lennartson, A. Roffey, K. Moth-Poulsen, *Tetrahedron Lett.* **2015**, *56*, 1457 – 1465.
[6] a) Z. Yoshida, *J. Photochem.* **1985**, *29*, 27 – 40; b) T. J. Kucharski, Y. Tian, S. Akbulatov, R. Boulatov, *Energy Environ. Sci.* **2011**, *4*, 4449 – 4472.
[7] a) A. D. Dubonosov, V. A. Bren, V. A. Chernoivanov, *Russ. Chem. Rev.* **2002**, *71*, 917 – 927; b) V. A. Bren', A. D. Dubonosov, V. I. Minkin, V. A. Chernoivanov, *Russ. Chem. Rev.* **1991**, *60*, 451 – 469.
[8] a) G. S. Hammond, N. J. Turro, A. Fischer, *J. Am. Chem. Soc.* **1961**, *83*, 4674 – 4675; b) X. An, Y. Xie, *Thermochim. Acta* **1993**, *220*, 17 – 25.
[9] a) K. Hirao, A. Ando, T. Hamada, O. Yonemitsu, *J. Chem. Soc. Chem. Commun.* **1984**, 300 – 302; b) V. I. Minkin, V. A. Breit, V. A. Chernoivanov, A. D. Dubonosov, S. V. Galichev, *Mol. Cryst. Liq. Cryst.* **1994**, *246*, 151 – 154; c) V. Gray, A. Lennartson, P. Ratanalert, K. Börjesson, K. Moth-Poulsen, *Chem. Commun.* **2014**, *50*, 5330 – 5332.
[10] M. Quant, A. Lennartson, A. Dreos, M. Kuisma, P. Erhart, K. Börjesson, K. Moth-Poulsen, *Chem. Eur. J.* **2016**, *22*, 13265 – 13274.
[11] a) J. Orrego-Hernández, A. Dreos, K. Moth-Poulsen, *Acc. Chem. Res.* **2020**, *53*, 1478 – 1487; b) M. Mansø, A. U. Petersen, Z. Wang, P. Erhart, M. B. Nielsen, K. Moth-Poulsen, *Nat. Commun.* **2018**, *9*, 1945; c) M. Kuisma, A. Lundin, K. Moth-Poulsen, P. Hyldgaard, P. Erhart, *ChemSusChem* **2016**, *9*, 1786 – 1794.
[12] Z. Wang, A. Roffey, R. Losantos, A. Lennartson, M. Jevric, A. U. Petersen, M. Quant, A. Dreos, X. Wen, D. Sampedro, K. Börjesson, K. Moth-Poulsen, *Energy Environ. Sci.* **2019**, *12*, 187 – 193.
[13] D. J. Cole-Hamilton, R. P. Tooze, *Catalyst separation, recovery and recycling. Chemistry and process design, Catalysis by Metal Complexes, Vol. 30*, Eds. D. J. Cole-Hamilton, R. P. Tooze, Springer, Dordrecht, **2006**, pp. 1 – 8.
[14] a) T. Luchs, M. Sarcletti, L. Zeininger, L. Portilla, C. Fischer, S. Harder, M. Halik, A. Hirsch, *Chem. Eur. J.* **2018**, *24*, 13589 – 13595; b) M. Sarcletti, D. Vivod, T. Luchs, T. Rejek, L. Portilla, L. Müller, H. Dietrich, A. Hirsch, D. Zahn, M. Halik, *Adv. Funct. Mater.* **2019**, *29*, 1805742.
[15] L. Zeininger, L. M. S. Stiegler, L. Portilla, M. Halik, A. Hirsch, *ChemistryOpen* **2018**, *7*, 282 – 287.
[16] a) S. Klein, T. Luchs, A. Leng, L. V. R. Distel, W. Neuhuber, A. Hirsch, *Bioengineering* **2020**, *7*, 126; b) C. K. Kim, P. Ghosh, C. Pagliuca, Z.-J. Zhu, S. Menichetti, V. M. Rotello, *J. Am. Chem. Soc.* **2009**, *131*, 1360 – 1361.
[17] a) A.-H. Lu, E. L. Salabas, F. Schüth, *Angew. Chem. Int. Ed.* **2007**, *46*, 1222 – 1244; *Angew. Chem.* **2007**, *119*, 1242 – 1266; b) R. B. N. Baig, R. S. Varma, *Chem. Commun.* **2013**, *49*, 752 – 770.
[18] T. Luchs, P. Lorenz, A. Hirsch, *ChemPhotoChem* **2020**, *4*, 52 – 58.
[19] a) J. Manassen, *J. Catal.* **1970**, *18*, 38 – 45; b) H. Wilson, R. Rinker, *J. Catal.* **1976**, *42*, 268 – 274; c) M. Chen, H. Feder, *J. Catal.* **1978**, *55*, 105 – 107; d) K. Maruyama, H. Tamiaki, *Chem. Lett.* **1982**, *11*, 1699 – 1702.
[20] M. Jevric, A. U. Petersen, M. Mansø, S. Kumar Singh, Z. Wang, A. Dreos, C. Sumby, M. B. Nielsen, K. Börjesson, P. Erhart, K. Moth-Poulsen, *Chem. Eur. J.* **2018**, *24*, 12767 – 12772.
[21] a) R. Hoffmann, *Acc. Chem. Res.* **1971**, *4*, 1 – 9; b) M. B. Robin, N. A. Kuebler, *J. Chem. Phys.* **1966**, *44*, 2664 – 2671.
[22] C. G. Hatchard, C. A. Parker, *Proc. R. Soc. London Ser. A* **1956**, *235*, 518 – 536.
[23] A. Dreos, Z. Wang, J. Udmark, A. Ström, P. Erhart, K. Börjesson, M. B. Nielsen, K. Moth-Poulsen, *Adv. Energy Mater.* **2018**, *8*, 1703401.
[24] K. Maruyama, H. Tamiaki, *J. Org. Chem.* **1986**, *51*, 602 – 606.
[25] H. Taoda, K. Hayakawa, K. Kawase, *J. Chem. Eng. Jpn.* **1987**, *20*, 335 – 338.
[26] a) R. Díaz-Torres, S. Alvarez, *Dalton Trans.* **2011**, *40*, 10742 – 10750; b) S. Alvarez, *Chem. Eur. J.* **2020**, *26*, 4350 – 4377.
[27] M. Quant, A. Hamrin, A. Lennartson, P. Erhart, K. Moth-Poulsen, *J. Phys. Chem. C* **2019**, *123*, 7081 – 7087.

Manuscript received: December 21, 2020
Revised manuscript received: January 14, 2021
Accepted manuscript online: January 15, 2021
Version of record online: February 22, 2021